Influence of electromechanical effects and wetting layers on band structures of AlN/GaN quantum dots and spin control

Sanjay Prabhakar[1] and Roderick Melnik[1,2,a)]
[1]*M^2 NeT Laboratory, Wilfrid Laurier University, 75 University Avenue West, Waterloo, Ontario N2L 3C5, Canada*
[2]*BCAM, Bizkaia Technology Park, 48160 Derio, Spain*

(Received 15 June 2010; accepted 30 July 2010; published online 30 September 2010)

In a series of recent papers we demonstrated that coupled electromechanical effects can lead to pronounced contributions in band structure calculations of low dimensional semiconductor nanostructures (LDSNs) such as quantum dots (QDs), wires, and even wells. Some such effects are essentially nonlinear. Both strain and piezoelectric effects have been used as tuning parameters for the optical response of LDSNs in photonics, band gap engineering, and other applications. However, the influence of spin orbit effects in presence of external magnetic field on single and vertically coupled QD has been largely neglected in the literature. The electron spin splitting terms which are coupled to the magnetic field through the Pauli spin matrix in these QDs become important in the design of optoelectronic devices as well as in tailoring properties of QDs in other applications areas. At the same time, single and vertically stacked QDs are coupled with electromagnetic and mechanical fields which become increasingly important in many applications of LDSN-based systems, in particular, where spin splitting energy is important. These externally applied electric and magnetic fields as well as the separation between the vertically coupled QDs can be used as tuning parameters. Indeed, as electromagnetic and elastic effects are often significant in LDSNs, it is reasonable to expect that the externally applied magnetic fields oriented along a direction perpendicular to the plane of two-dimensional electron gas in the QDs may also be used as a tuning parameter in the application of light emitting diodes, logic devices, for example, OR gates, AND gates and others. In this paper, by using the fully coupled model of electroelasticity, we analyze the influence of these effects on optoelectronic properties of QDs. Results are reported for III–V type semiconductors with a major focus given to AlN/GaN based QD systems. © *2010 American Institute of Physics*. [doi:10.1063/1.3485602]

I. INTRODUCTION

Single electron spins can be manipulated through the active modification in the spin orbit interaction formed in the plane of a two-dimensional electron gas (2DEG) in quantum dots (QDs) (Refs. 1 and 2) that has received considerable attention for potential use in noncharge-based logic devices, solid state quantum computing.[3–14]

Wide band gap semiconductor materials such as AlN/GaN QDs have attracted significant attention due to their current and potential applications in optical, optoelectronic, and electronic devices used in nano- and bionanotechnological applications. Strongly coupled self-assembled QDs are grown either in the same wetting layer or a vertically stack of closely spaced layers. Single and vertically stacked double QDs grown by Stranski–Krastanov process are of special interest because of its potential applications in QDs lasers, light emitting diodes as qubits for quantum computation, and other applications.[15–24]

Strain is induced due to the lattice mismatch at the interfaces between two different types of semiconductors which can be used as a tuning parameter in tailoring the electronic and optical properties of single and multiple self-assembled QDs.[25–29] Various approaches such as atomistic, pseudopotential, and tight binding have been applied to investigate the optical and electronic properties of such nano-objects.[21,30–33]

In this paper, we present a numerical analysis of the band structure of single and vertically stacked double AlN/GaN QDs under the influence of electroelasticity. By using the finite element method (FEM), we study the effect of electroelasticity on the electronic properties of truncated AlN/GaN QDs in the presence of wetting layers (WLs). Effect of several parameters such as electromechanical fields, magnetic fields, and coefficient of spin orbit interaction on the eigenvalues and wave functions of single and vertically stacked double QDs have been reported.

The key parameters in controlling the electron spin in a single and vertically stacked double QDs are the Rashba[34] spin orbit couplings. The Rashba spin orbit coupling arises from the structural inversion asymmetry of the triangle shaped quantum well confining potential along z-direction as shown in Figs. 1(b) and 7(a). The mathematical expressions for these interaction is given in Eq. (17) and are well established for semiconductor heterojunction-type devices.[11–14]

It is also generally understood that the Zeeman spin splitting energy depends on the direction of an applied magnetic field.[35–38] In the present work we only consider the magnetic fields along a direction normal to the plane of

a)Electronic mail: rmelnik@wlu.ca.

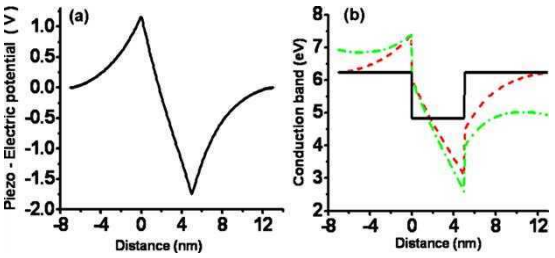

FIG. 1. (Color online) The influence of piezoelectric potential on the flat band diagram of AlN/GaN conduction band. (a) Piezoelectric field along z-direction at $\rho=0$ and (b) effect of piezoelectric potential on the conduction band of AlN/GaN QD along z-direction at $\rho=0$. In (b), we use the externally applied electric fields $F_z=10^4$ V/cm (dashed line) and $F_z=10^6$ V/cm (dashed-dotted line) as an extra term on the conduction band diagram (solid line) including piezoelectric potential and $\alpha_R=5\times10^{-4}$ eV nm as a Rashba coefficient value.

2DEG. In several recent works, Rashba spin orbit effects in a QD systems were explored.[39–41] A subject that seems to have studied a little in AlN/GaN QD, however, is the question of piezoelectric effects in single and vertically stacked double QDs and is the subject of the present investigation. Our approach is most closely related to that of Refs. 30 and 42 but differs in a sense that we include the Rashba spin orbit effects into the Hamiltonian and take a numerical approach based on the FEM (Ref. 43), whereas the authors of Refs. 30 and 42 did not consider the Rashba spin orbit coupling. We now turn to a discussion of our model, followed by a brief description of our computation methodology.

II. MATHEMATICAL MODEL FOR COUPLING CLASSICAL AND QUANTUM MECHANICAL PARTS

Electromechanical balance equations for wurtzite (WZ) structures are axisymmetric. Therefore, the original three-dimensional problem can be reduced to a 2D problem. The coupled equations of WZ structure in the presence of electromechanical effects in cylindrical coordinates can be written as[44]

$$\frac{\partial\sigma_{\rho\rho}}{\partial\rho}+\frac{\partial\sigma_{\rho z}}{\partial z}+\frac{\sigma_{\rho\rho}-\sigma_{\phi\phi}}{\rho}=0, \tag{1}$$

$$\frac{\partial\sigma_{\rho z}}{\partial\rho}+\frac{\partial\sigma_{zz}}{\partial z}+\frac{1}{\rho}\sigma_{\rho z}=0, \tag{2}$$

$$\frac{\partial D_{\rho}}{\partial\rho}+\frac{\partial D_{z}}{\partial z}+\frac{1}{\rho}D_{\rho}=0. \tag{3}$$

The stress tensor components and the electric displacement vector components can be written as

$$\sigma_{\rho\rho}=C_{11}\varepsilon_{\rho\rho}+C_{12}\varepsilon_{\phi\phi}+C_{13}\varepsilon_{zz}+e_{31}\partial_z V, \tag{4}$$

$$\sigma_{\phi\phi}=C_{11}\varepsilon_{\phi\phi}+C_{12}\varepsilon_{\rho\rho}+C_{13}\varepsilon_{zz}+e_{31}\partial_z V, \tag{5}$$

$$\sigma_{\rho z}=2C_{44}\varepsilon_{\rho z}+e_{15}\partial_\rho V, \tag{6}$$

$$\sigma_{zz}=C_{13}\varepsilon_{\rho\rho}+C_{13}\varepsilon_{\phi\phi}+C_{33}\varepsilon_{zz}+e_{33}\partial_z V, \tag{7}$$

$$D_{\rho}=2e_{15}\varepsilon_{\rho z}-\epsilon_1\partial_\rho V, \tag{8}$$

$$D_z=e_{31}(\varepsilon_{rr}+\varepsilon_{\phi\phi})e_{33}\varepsilon_{zz}-\epsilon_3\partial_z V+P_z^{sp}, \tag{9}$$

where C_{kl} is the elastic moduli constant, e_{ij} is the piezoelectric constant, ϵ_{in} is the permittivity, V is the piezoelectric potential, and $E=-(\partial V/\partial z)$ is the built in piezoelectric field. Equations (1)–(9) is a system of coupled electroelasticity which, in a more general dynamic setting, was studied in Refs. 44 and 45, where for the first time a mathematical justification of this model well-posedness was obtained with further results on differential-variational numerical approximations and a generalization of the Courant–Fridrichs–Lewy stability condition found in Refs. 46 and 47. Those early results demonstrated the importance of the fully coupled approach in dealing with problems of electroelasticity, when one needs to account for the piezoelectric effect. Indeed, although still used by a number of authors, the minimization of pure elastic, rather than the full electroelastic, energy in problems like this may lead to substantial errors, in particular in the context of modeling low dimensional nanostructures.[26] Furthermore, the coupled solution in the latter case becomes especially important due to a fact that, in contrast to many classical problems, we need here to account for the lattice mismatch between different materials involved or the internal strain. Among other things, the internal strain may lead to a reduced band gap in low dimensional nanostructures and may partially counter the quantum confinement effect (e.g., Ref. 48). The idea to account for such a strain has been developed on the basis of the general theory for anisotropic elastic media which goes back to early works of Lifshits and Rosentsveig[49] (see also references in Ref. 50). The theory was developed and applied to nanostructure modeling by a number of authors.[26,30,42,51–53] In what follows, we apply the same theory and present the total strain tensor, accounting for both the standard Cauchy strain and the internal strain due to lattice mismatch, that is,

$$\varepsilon_{ij}=\varepsilon_{ij}^{(u)}+\varepsilon_{ij}^{(0)}, \tag{10}$$

with the Cauchy strain and the internal strain components defined by

$$\varepsilon_{ij}^{(u)}=(\partial_j u_i+\partial_i u_j)/2, \quad \varepsilon_{ij}^{(0)}=(\delta_{ij}-\delta_{il}\delta_{jl})\varepsilon_a^*+\delta_{il}\delta_{jl}\varepsilon_c^*, \tag{11}$$

respectively. In our case we have

$$\varepsilon_{\rho\rho}=\frac{\partial u_\rho}{\partial\rho}+\varepsilon_a^\star, \quad \varepsilon_{zz}=\frac{\partial u_z}{\partial z}+\varepsilon_c^\star, \tag{12}$$

$$\varepsilon_{\phi\phi}=\frac{u_\rho}{\rho}+\varepsilon_a^\star, \quad \varepsilon_{\rho z}=\frac{1}{2}\left(\frac{\partial u_\rho}{\partial z}+\frac{\partial u_z}{\partial\rho}\right). \tag{13}$$

Here, $\varepsilon_a^\star=(a_m-a_{\mathrm{QD}}/a_m)$ and $\varepsilon_c^\star=(c_m-c_{\mathrm{QD}}/c_m)$ are the local intrinsic strains along a- and c-directions, respectively (which are nonzero in the dot and zero otherwise). Also, a_m, c_m and a_{QD}, c_{QD} are the lattice constants of the matrix and the QD, respectively.

We consider the motion of the electron confined along the z-direction in presence of magnetic field oriented along a direction perpendicular to the plane of 2DEG. Our approach closely related to that of Ref. 30, however we consider the

Rashba spin orbit effect as an extra term in the single conduction band model. Therefore, the total Hamiltonian for the conduction band can be written as

$$H = H_{xyz} + H_e^{\varepsilon} + H_R. \tag{14}$$

Here, H_e^{ε} is the strain dependent part of the kinetic energy of the electron and H_R is the Rashba–Bychkov spin orbit interaction to be discussed later. The remaining portion of the Hamiltonian can be written as,

$$H_{xyz} = P_x \frac{1}{m_e^{\perp}} P_x + P_y \frac{1}{m_e^{\perp}} P_y + P_z \frac{1}{m_e^{\parallel}} P_z + E_c(r_e) + eV(r_e) + eF_z z + \frac{1}{2} g_0 \mu_B B \sigma_z, \tag{15}$$

where the kinetic momentum operator $\vec{P} = \vec{p} + (e/c)\vec{A}$ is the sum of the conical momentum operator $\vec{p} = -i\hbar(\partial_x, \partial_y, 0)$ and $\vec{A} = (B/2)(-y, x, 0)$ which is the vector potential in symmetric gauge. Here, B is the applied magnetic field along z-direction, μ_B is the Bohr magneton, $E_c(r_e)$ is the conduction band edge profile and e is the electronic charge. We denote σ_z the usual Pauli spin matrix along z-direction and g_0 is the bulk g-factor for AlN and GaN materials. Since our aim is to control the electron spin in AlN/GaN QD with the application of gate potentials, we consider the distortion potential $eF_z z$ pointing along c-axis as an extra term in the conduction band. Here F_z is the externally applied electric field along z-direction which is different than the built in piezoelectric field E.

The strain dependent part of the electron Hamiltonian in Eq. (14) can be written as

$$H_e^{\varepsilon} = a_c^{\parallel}(r)\varepsilon_{zz}(r) + a_c^{\perp}(r)[\varepsilon_{xx}(r) + \varepsilon_{yy}(r)], \tag{16}$$

where $a_c^{\parallel}$ and $a_c^{\perp}$ are the conduction band deformation potentials along the symmetric and perpendicular to the symmetric axis. In cylindrical coordinates, we can write $\varepsilon_{xx} + \varepsilon_{yy} = \partial u_\rho/\partial\rho + u_\rho/\rho + 2\varepsilon_a^{\star}$.

Lastly, we consider the Hamiltonian associated with Rashba spin orbit interaction that is embodied in the Hamiltonian H. This spin orbit interaction is the essential ingredient in the phenomena of switching electron spin with gate potentials.[2,10,11,34,35] We have

$$H_R = \frac{\alpha_R}{\hbar}(\sigma_x P_y - \sigma_y P_x), \tag{17}$$

where α_R is the Rashba coefficients for spin orbit interaction, σ_x and σ_y are the usual Pauli spin matrices along x- and y-directions. Rashba spin orbit interaction and the magnetic field oriented along a direction perpendicular to the plane of 2DEG preserve the axial symmetry.[39–41] Because the total Hamiltonian in Eq. (14) commutes with the z-projection of the total momentum operator,[41]

$$j_z = l_z + \tfrac{1}{2}\sigma_z, \quad \text{where} \quad l_z = -i\partial_\phi. \tag{18}$$

Here, the total momentum operator, $j = \pm(1/2)m$ and $m = 1, 2, 3, \ldots$. The eigenfunctions of the total Hamiltonian operator H in Eq. (14) can be written as[39–41]

$$\psi_j(\rho, \phi, z) = \begin{bmatrix} e^{i(j-(1/2))\phi} f_j(\rho, z) \\ e^{i(j+(1/2))\phi} g_j(\rho, z) \end{bmatrix}, \tag{19}$$

where f_j and g_j are the components of the total wave function. The total Hamiltonian H for the conduction band can be written in cylindrical coordinates by substituting the components of Eq. (19) into Eq. (14) [see Eq. (A1)]. The details procedure are also mentioned in the Ref. 41. So, we can write

$$H = \begin{bmatrix} h_+ & \alpha_R\left[\frac{\partial}{\partial\rho} + \frac{1}{\rho}\left(j + \frac{1}{2}\right) + \frac{eB\rho}{2\hbar}\right] \\ \alpha_R\left[-\frac{\partial}{\partial\rho} + \frac{1}{\rho}\left(j - \frac{1}{2}\right) + \frac{eB\rho}{2\hbar}\right] & h_- \end{bmatrix}, \tag{20}$$

where

$$h_{\pm} = -\frac{\hbar^2}{2m_0}\left[\frac{1}{\rho}\frac{\partial}{\partial\rho}\frac{\rho}{m_e^{\perp}}\frac{\partial}{\partial\rho} + \frac{\partial}{\partial z}\frac{1}{m_e^{\parallel}}\frac{\partial}{\partial z} - \frac{1}{\rho^2}\frac{1}{m_e^{\perp}}\left(j \mp \frac{1}{2}\right)^2\right] + \frac{1}{8}m_e^{\perp}\omega_c^2\rho^2 + \frac{\hbar\omega_c}{2}\left(j \mp \frac{1}{2}\right) \mp \frac{1}{2}g_0\mu_B B + E_c + eF_z z + eV + a_c^{\parallel}\varepsilon_{zz} + a_c^{\perp}\left(\frac{\partial u_r}{\partial r} + \frac{u_r}{r} + 2\varepsilon_a^{\star}\right), \tag{21}$$

where $\omega_c = (eB/m_e^{\perp}c)$ is the cyclotron frequency [see Eq. (A1)], $m_e^{\perp}$ and $m_e^{\parallel}$ are the effective masses. Here, we consider the experimentally reported bulk $g_0 = 1.9885$ for AlN material and bulk $g_0 = 1.9510$ for GaN material from the Ref. 54.

The eigenvalue equation

$$H|\psi_j(\rho, z)\rangle = \epsilon|\psi_j(\rho, z)\rangle, \tag{22}$$

with H in cylindrical coordinates given by Eq. (20) satisfies the following system of second order differential equations

$$(h_+ - \epsilon)f_j + \alpha_R\left[\frac{\partial}{\partial\rho} + \frac{1}{\rho}\left(j + \frac{1}{2}\right) + \frac{eB\rho}{2\hbar}\right]g_j = 0, \tag{23}$$

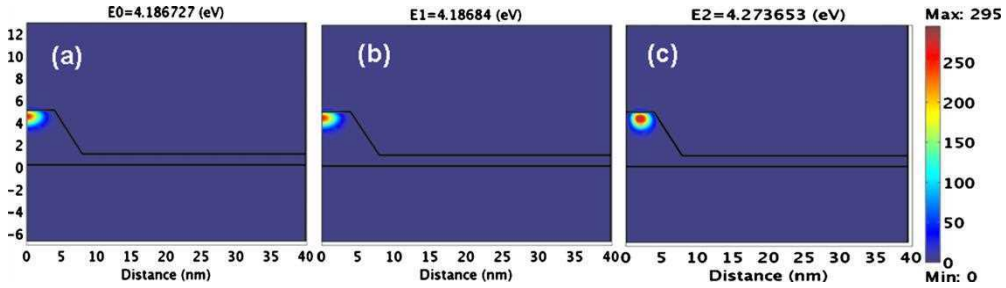

FIG. 2. (Color online) The three lowest eigenvalues and wave functions of the electrons in the conduction band of AlN/GaN QD in the potential that has been considered in (b) (dashed line). These eigenstates and eigenvalues have been found by solving Eq. (20). In (a), we consider $j=-1/2$ which gives the ground state while $j=1/2$ and $-3/2$ give first and second excited states that is shown in (b) and (c). Here, we consider the electric field $F_z=10^4$ V/cm, magnetic field 1 T and $\alpha_R=5\times10^{-4}$ eV nm as a Rashba coefficient value.

$$\alpha_R\left[-\frac{\partial}{\partial\rho}+\frac{1}{\rho}\left(j-\frac{1}{2}\right)+\frac{eB\rho}{2\hbar}\right]f_j+(h_- -\epsilon)g_j=0. \qquad (24)$$

The differential Eqs. (23) and (24) were solved numerically to obtain the lowest few eigenvalues and eigenstates with respect to the various parameters of the system. These parameters include the magnetic field strength B, the electric field F_z, the strength of Rashba coefficient α_R and the separation between the two vertically stacked double QDs. The analytical solution of such differential equations is available in some special simplified cases, e.g., Ref. 41.

Results for the variation in spin splitting energy to the magnetic field in the piezoelectric potential by FEM are described in the following section by solving the coupled Schrödinger Eqs. (23) and (24).

III. RESULTS AND DISCUSSIONS

We utilize a multiphysics simulation strategy based on the FEM (Ref. 43) to provide a realistic description of the conduction band diagram of AlN/GaN QD. The idea is to solve the coupled of Eq. (1) through Eq. (3) in cylindrical coordinates to get the realistic piezoelectric potential and piezoelectric strain. In the first step of our approach, we plotted the piezoelectric field along z-direction in AlN/GaN QDs at $\rho=0$ as shown in Fig. 1(a). We add this piezoelectric potential into the flat band diagram of AlN/GaN QD as shown in Fig. 1(b) (black-continuous line) and considered externally applied electric fields of 10^4 and 10^6 V/cm as an extra term as shown in Fig. 1(b) (red—dashed and green—dashed-dotted). Finally, we plotted these potentials along z-direction at $\rho=0$ as shown in Fig. 1(b). From these plots, we see that we can easily modify the band diagram by applied gate potentials which is essential ingredient in controlling the electron spin and can be discussed in more details latter in this section. These are consistent results that was found in the literature in Refs. 27 and 53.

Finally, we solve the coupled Schrödinger Eqs. (23) and (24) in the potential of Fig. 1(b) (red—dashed) at $F_z=10^4$ V/cm to get the wave functions of the three lowest eigenvalues as shown in Fig. 2. Here we estimated that ground state eigenvalue is 4.186 727 eV associated with the total angular momentum $j=-1/2$ and the first excited state eigenvalue is 4.186 840 eV associated with the total angular momentum $j=1/2$. Similarly, the third excited state eigenvalue is 4.273 653 eV associated with the total angular momentum of $j=-3/2$. We can change these eigenvalues with the help of gate potentials in presence of magnetic field and thus spin splitting energy can be easily moved from either higher eigenvalues to the lower eigenvalues and vice versa. These movement of eigenvalues will be described in more details later in this section.

We now turn to a presentation of another important result of this work: the spin splitting energy of ground and first excited states through the application of magnetic and electric fields.

In the absence of the magnetic field, as it clear from Eq. (20) that there is an additional asymmetry at $j_z\rightarrow -j_z$ due to time inversion. It means, the eigenstates with the projection of total angular momentum equal to j and $-j$ are Kramers degenerate. We find the ground state and first excited state Kramers degenerate eigenvalues at 4.186 728 and 4.388 569 eV by directly solving the coupled Schrödinger Eqs. (23) and (24) which is shown in Fig. 3. Here we consider $j=1/2$ in Eq. (23) and $-j=1/2$ in Eq. (24). In presence of magnetic field, the Kramers degeneracy lifted into the spin splitting energy and its value increases with the increase in magnetic field. In Fig. 3, we plotted the spin splitting energy of the ground and first excited state versus the magnetic field associated with the total angular momentum $j=1/2$ (triangle pointing up—black) and $j=-1/2$ (triangle pointing down—red). We found that the divergence in the spin splitting energy increases with the increase in magnetic field due to the Rashba effect. Here we consider the externally applied elec-

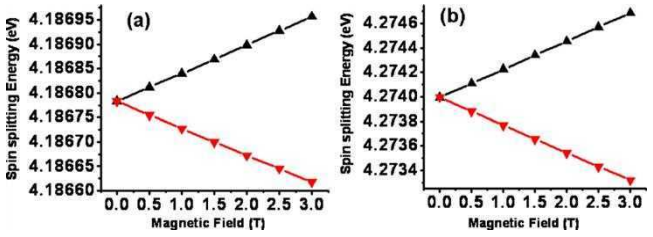

FIG. 3. (Color online) The spin splitting energy between two lowest eigenstates vs magnetic field in two different cases: (a) the ground state energy of spin down electron for the quantum number $j=1/2$ (triangle pointing up) and ground state energy of spin up electron for the quantum number $j=-1/2$ (triangle pointing down). (b) First excited state energy of spin down electron for the quantum number $j=1/2$ (triangle pointing up) and first excited state energy of spin up electron for the quantum number $j=-1/2$ (triangle pointing down). Here, we consider the electric field, $F_z=10^4$ V/cm as an extra term in the piezoelectric potential of Fig. 1(b) (dash red) and $\alpha_R=5\times10^{-4}$ eV nm as the Rashba coefficient value.

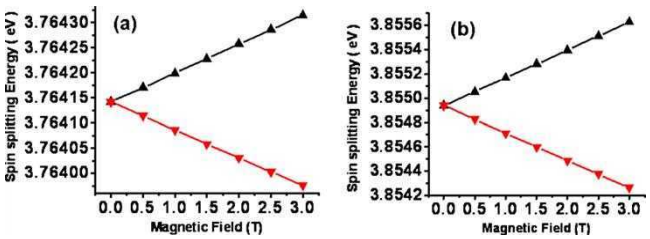

FIG. 4. (Color online) The spin splitting energy between two lowest eigen states vs magnetic field in two different cases: (a) the ground state energy of spin down electron for the quantum number $j=1/2$ (triangle pointing up) and ground state energy of spin up electron for the quantum number $j=-1/2$ (triangle pointing down). (b) First excited state energy of spin down electron for the quantum number $j=1/2$ (triangle pointing up) and first excited state energy of spin up electron for the quantum number $j=-1/2$ (triangle pointing down). Here, we consider the electric field, $F_z=10^6$ V/cm as an extra term in the piezoelectric potential of Fig. 1(b) (solid line) and $\alpha_R=5\times10^{-4}$ eV nm as the Rashba coefficient value.

tric field, $F_z=10^4$ V/cm as an extra term in the piezoelectric potential of Fig. 1(b) (dashed—red) and solved the Schrödinger Eqs. (23) and (24) to get the ground state eigenvalues for $j=1/2$ and $j=-1/2$. We keep the Rashba coefficient value, $\alpha_R=5\times10^{-4}$ eV nm.

The spin splitting energy can be easily moved to the lower energy states or vice versa by applying suitable gate potentials. Here we show that by introducing external applied electric field, $F_z=10^6$ V/cm in Fig. 1(b) (dashed-dotted—green), one can move the Kramers degeneracy by 3.764 142 eV in the confining potential in Fig. 1(b) (dashed-dotted—green). The numerical simulation results for the spin splitting energy vs magnetic field in the above potential are shown in Fig. 4. Controlling eigenvalues more precisely with the help of gate potentials can lead to the design of spin based logic devices.

Finally, we plotted the spin splitted energy difference of the ground and first excited state versus magnetic field as shown in Fig. 5. Here we consider the externally applied electric field, $F_z=10^4$ V/cm as an extra term in the piezoelectric potential of Fig. 1(b) (dashed—red) and solved the Schrödinger Eqs. (23) and (24) to get the ground state eigen-

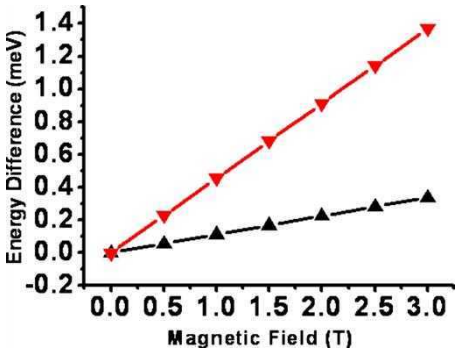

FIG. 5. (Color online) The spin splitting energy difference vs magnetic field for two different cases: (a) the spin splitting energy difference of the ground state of spin down electron ($j=-1/2$) and spin up electron ($j=1/2$) (triangle pointing up) and (b) the spin splitting energy difference of the first excited state of spin down electron ($j=-1/2$) and spin up electron ($j=1/2$) (triangle pointing down). Here, we consider the electric field, $F_z=10^4$ V/cm as an extra term in the piezoelectric potential of Fig. 1(b) (continuous line) and $\alpha_R=5\times10^{-4}$ eV nm as the Rashba coefficient value.

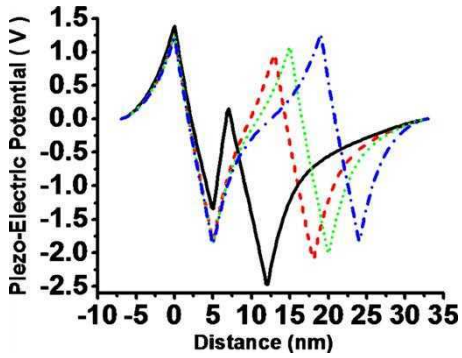

FIG. 6. (Color online) Effect of piezoelectric potential on two vertically stacked double AlN/GaN QDs along z-direction at $\rho=0$. Here, we take the distance between two vertically stacked double QDs as (2, 6, 10, and 14) nm (solid line, dashed line, dotted line, and dashed-dotted line).

values for $j=1/2$ and $j=-1/2$. We keep the Rashba coefficient value, $\alpha_R=5\times10^{-4}$ eV nm. We see that the ground state spin splitting energy varies with a slope of 0.114 with the increase in magnetic field as shown in Fig. 5 (triangle pointing up—black). However, the first excited state spin splitting energy varies with a slope of 0.454 with the increase in magnetic field as shown in Fig. 5 (triangle pointing down—red). It means, the Rashba spin orbit interaction for the first excited state is approximately one half order of magnitude stronger than the ground state.

Lastly, we consider the distance between two vertically coupled AlN/GaN QDs as a tuning parameter in controlling the electron spin. Figure 7(a) is the conduction band edge profile along the z-direction at $\rho=0$ including piezoelectric potential. Here, we consider the electric filed $F_z=10^4$ V/cm as an extra term in the conduction band of AlN/GaN QD. Here we observe the effect of piezoelectric potential in the conduction band of two vertically stacked double QDs. Polarization of charges due to piezoelectric effect is different in AlN/GaN layer than the GaN/AlN layer in the QDs as shown in Fig. 6 which gives different band offsets as well as different asymmetric quantum wells on vertically stacked double QDs along z-direction as shown in Fig. 7(a). Similar type of results have been reported in the Ref. 55 but here we consider the Rashba spin orbit interaction as well as piezoelectric effect in the conduction band diagram of AlN/GaN QD as an extra piece of information. However, the authors in Ref. 55 did not consider Rashba spin orbit interaction. Finally, we solve the coupled Schrödinger Eqs. (23) and (24) for the two vertically stacked double QDs in the piezoelectric potential of [Fig. 7(a)] (dashed—red and dashed-dotted—blue) to get the ground state eigenvalues and wave functions as shown in Figs. 7(b) and 7(c). We can predict that in vertically coupled QDs, different band offsets in the layer of AlN/GaN than the layer of GaN/AlN QDs change their properties with the variations in the distance between two vertically coupled QDs as shown in Fig. 7(a). It means, the localization of electron wave functions in vertically stacked double QDs depends on the separation between these dots. In Fig. 7(b), we observe that electron wave functions are localized to the upper QD if we keep the separation between the two vertically stacked QD is around 6 nm, pointing to the larger piezoelectric effect in the upper QD

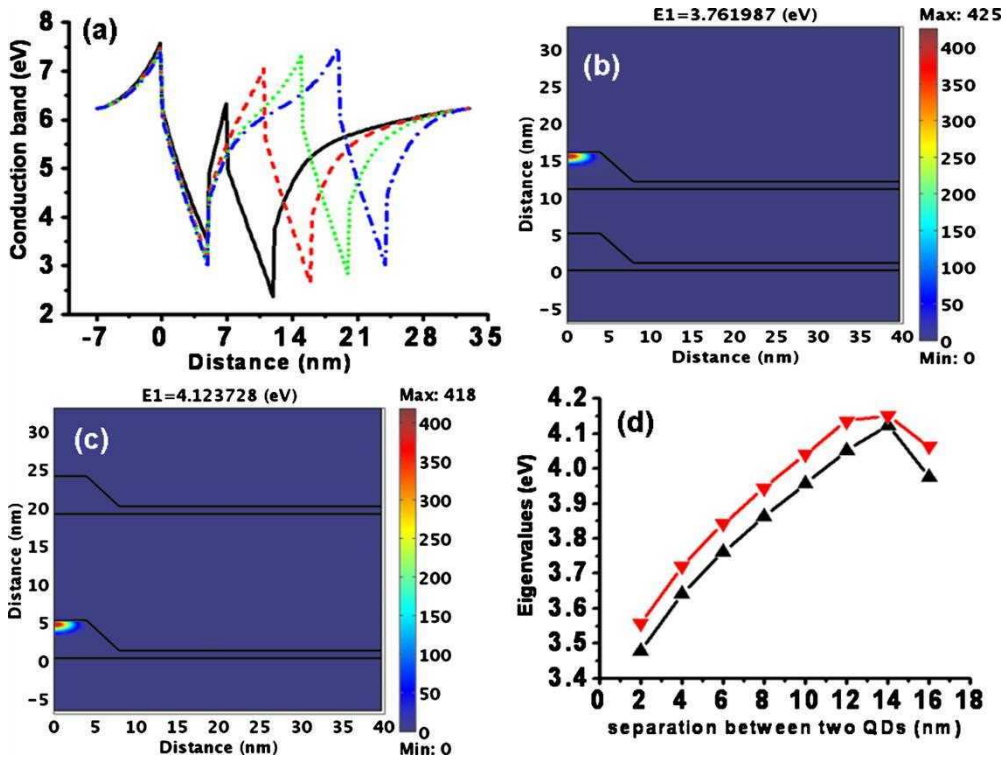

FIG. 7. (Color online) (a) Effect of piezoelectric potential on the conduction band of two vertically coupled AlN/GaN QDs along z-direction. Here we take the distance between two vertically coupled QDs as a tuning parameter (2, 6, 10, and 14) nm (solid line, dashed line, dotted line, and dashed-dotted line).[(b) and (c)] The ground state eigenvalues and wave functions on the conduction band of two vertically stacked double AlN/GaN QD in the potential that has been considered in (a) (dashed line and dashed-dotted line). These wave functions and eigenvalues have been found by solving Eqs. (23) and (24). (d) Ground state (triangle pointing up) and first excited states eigenvalues (triangle pointing down) that was found in the potential of (a) vs separation between the two QDs. Here, we consider $j=-1/2$ and the electric field $F_z=10^4$ V/cm, magnetic field 1 T and $\alpha_R=5\times10^{-4}$ eV nm as a Rashba coefficient value.

which is shown by the conduction band diagram in Fig. 7(a) (dashed—red). However, this effect is reduced with the increase in the separation between the two QDs as shown by the conduction band diagram in Fig. 7(a) (dashed-dotted—blue)and all electron wave functions are localized into the lower QD as shown in Fig. 7(c). Here, the separation between the two vertically stacked QDs is taken as 14 nm. One can easily vary the spin splitted ground state energy by the variation in the distance between the two vertically stacked QDs as shown in Fig. 7(d) which can be used as an additional tuning parameter in controlling the electron spin in the design of the spintronics devices.

IV. CONCLUSIONS

We have carried out a numerical simulation study of gate induced tunability of the spin splitted energy in an AlN/GaN QD. We accounted for piezoelectric effect on the band structure of single and double QDs in presence of spin orbit interaction and employed a coupled numerical approach to obtain the eigenvalues and eigenstates based on the FEM.

The key result of this work is illustrated in Figs. 3 and 5: spin splitting energy can be significantly changed with the increase in the electric field as well as the magnetic field. First, we analyzed the piezoelectric effects on the band structure of single and vertically stacked double AlN/GaN QDs with wetting layers in presence of spin orbit interaction. We found that the spin splitting energy can be changed from lower eigenvalues to higher eigenvalues and vice versa with the help of gate potentials. Similarly, we observed that the separation between the two coupled QDs can be used as an additional tuning parameter which could be quite important for such applications as the design of the spintronics logic devices. The spin splitted ground and first excited states can be modified by changing the separation between the two vertically stacked double QDs which is crucial in the applications areas mentioned.

ACKNOWLEDGMENTS

The authors acknowledges Dr. Eduard Takhtamirov for his many helpful discussions. This work was supported by NSERC and CRC program.

APPENDIX: HAMILTONIAN IN CYLINDRICAL COORDINATES

In cylindrical polar coordinates, we have $x=\rho\cos\phi$, $y=\rho\sin\phi$, and $z=z$. According to chain rule, we can write

$$\frac{\partial}{\partial x}=\cos\phi\frac{\partial}{\partial\rho}-\frac{\sin\phi}{\rho}\frac{\partial}{\partial\phi}, \tag{A1}$$

$$\frac{\partial}{\partial y}=\sin\phi\frac{\partial}{\partial\rho}+\frac{\cos\phi}{\rho}\frac{\partial}{\partial\phi}, \tag{A2}$$

where $\tan\phi = y/x$ and $\rho = \sqrt{x^2+y^2}$. With the help of Eqs. (A1) and (A2), the Hamiltonian Eq. (15) can be written in cylindrical coordinates as

$$H_{xyz} = -\frac{\hbar^2}{2m_0}\left[\frac{1}{\rho}\frac{1}{\partial\rho}\left(\frac{\rho}{m_e^{\perp}}\frac{\partial}{\partial\rho}\right) + \frac{1}{\rho^2}\frac{1}{m_e^{\perp}}\frac{\partial^2}{\partial\phi^2}\right] - \frac{\hbar^2}{2m_0}\frac{\partial}{\partial z}\left(\frac{1}{m_e^{\parallel}}\frac{\partial}{\partial z}\right) - \frac{i\hbar\omega_c}{2}\frac{\partial}{\partial\phi} + \frac{1}{8}m_e^{\perp}\omega_c^2\rho^2 + E_c(r_e) + eV(r_e) + eF_z z + \frac{1}{2}g_0\mu_B B\sigma_z, \tag{A3}$$

where $m_e^{\perp}$ and $m_e^{\parallel}$ are the effective masses and $\omega_c = (eB/m_e^{\perp}c)$ is the cyclotron frequency. Also, with the help of Eqs. (A1) and (A2), the Hamiltonian (17) can be written in cylindrical coordinates as

$$H_R = \begin{bmatrix} 0 & \alpha_R e^{-i\phi}\left[\frac{\partial}{\partial\rho} - \frac{i}{\rho}\frac{\partial}{\partial\phi} + \frac{eB\rho}{2\hbar}\right] \\ \alpha_R e^{i\phi}\left[-\frac{\partial}{\partial\rho} - \frac{i}{\rho}\frac{\partial}{\partial\phi} + \frac{eB\rho}{2\hbar}\right] & 0 \end{bmatrix}. \tag{A4}$$

Finally, the strain dependent part of the electron Hamiltonian (16) can be written in cylindrical coordinates as

$$H_e^{\varepsilon} = a_c^{\parallel}(r)\varepsilon_{zz}(r) + a_c^{\perp}(r)\left[\frac{\partial u_\rho}{\partial\rho} + \frac{u_\rho}{\rho} + 2\varepsilon_a^{\star}\right]. \tag{A5}$$

By substituting the components of Eq. (19) into Eqs. (A3)–(A5), we get the total Hamiltonian H in cylindrical coordinates which was written in Eq. (20).

[1] M. Governale, Phys. Rev. Lett. **89**, 206802 (2002).
[2] S. Prabhakar and J. E. Raynolds, Phys. Rev. B **79**, 195307 (2009).
[3] H.-A. Engel, L. P. Kouwenhoven, D. Loss, and C. M. Marcus, Quantum Inf. Process. **3**, 115 (2004).
[4] W. A. Coish and D. Loss, Phys. Rev. B **75**, 161302 (2007).
[5] D. D. Awschalom, D. Loss, and N. Samarth, *Semiconductor Spintronics and Quantum Computation* (Springer, Berlin, 2002).
[6] R. Hanson, L. P. Kouwenhoven, J. R. Petta, S. Tarucha, and L. M. K. Vandersypen, Rev. Mod. Phys. **79**, 1217 (2007).
[7] I. Žutić, J. Fabian, and S. D. Sarma, Rev. Mod. Phys. **76**, 323 (2004).
[8] S. Bandyopadhyay, Phys. Rev. B **61**, 13813 (2000).
[9] A. R. Trivedi and S. Bandyopadhyay, J. Appl. Phys. **103**, 104311 (2008).
[10] R. de Sousa and S. D. Sarma, Phys. Rev. B **68**, 155330 (2003).
[11] E. I. Rashba and A. L. Efros, Phys. Rev. Lett. **91**, 126405 (2003).
[12] E. A. Laird, C. Barthel, E. I. Rashba, C. M. Marcus, M. P. Hanson, and A. C. Gossard, Phys. Rev. Lett. **99**, 246601 (2007).
[13] C. S. Tang, A. G. Mal'shukov, and K. A. Chao, Phys. Rev. B **71**, 195314 (2005).
[14] A. L. Efros, E. I. Rashba, and M. Rosen, Phys. Rev. Lett. **87**, 206601 (2001).
[15] S. J. Pearton, C. R. Abernathy, M. E. Overberg, G. T. Thaler, D. P. Norton, N. Theodoropoulou, A. F. Hebard, Y. D. Park, F. Ren, J. Kim, and L. A. Boatner, J. Appl. Phys. **93**, 1 (2003).
[16] W. Shan, T. J. Schmidt, X. H. Yang, S. J. Hwang, J. J. Song, and B. Goldenberg, Appl. Phys. Lett. **66**, 985 (1995).
[17] B. Lin, Z. Fu, and Y. Jia, Appl. Phys. Lett. **79**, 943 (2001).
[18] A. Rubio, J. L. Corkill, M. L. Cohen, E. L. Shirley, and S. G. Louie, Phys. Rev. B **48**, 11810 (1993).
[19] Y. Kato, S. Kitamura, K. Hiramatsu, and N. Sawaki, J. Cryst. Growth **144**, 133 (1994).
[20] G. Yu, G. Wang, H. Ishikawa, M. Umeno, T. Soga, T. Egawa, J. Watanabe, and T. Jimbo, Appl. Phys. Lett. **70**, 3209 (1997).
[21] S. H. Park and S. L. Chuang, Appl. Phys. Lett. **72**, 3103 (1998).
[22] L. C. Lew Yan Voon, C. Galeriu, B. Lassen, M. Willatzen, and R. Melnik, Appl. Phys. Lett. **87**, 041906 (2005).
[23] B. Daudin, F. Widmann, G. Feuillet, Y. Samson, M. Arlery, and J. L. Rouvière, Phys. Rev. B **56**, R7069 (1997).
[24] F. Widmann, J. Simon, B. Daudin, G. Feuillet, J. L. Rouvière, N. T. Pelekanos, and G. Fishman, Phys. Rev. B **58**, R15989 (1998).
[25] S. R. Patil and R. V. N. Melnik, J. Phys. D: Appl. Phys. **42**, 145113 (2009).
[26] R. V. N. Melnik and R. Mahapatra, Comput. Struct. **85**, 698 (2007).
[27] S. R. Patil and R. V. N. Melnik, Nanotechnology **20**, 125402 (2009).
[28] R. V. N. Melnik and M. Willatzen, Nanotechnology **15**, 1 (2004).
[29] R. V. N. Melnik and K. N. Zotsenko, Modell. Simul. Mater. Sci. Eng. **12**, 465 (2004).
[30] V. A. Fonoberov and A. A. Balandin, J. Appl. Phys. **94**, 7178 (2003).
[31] W. Jaskólski, M. Zieliński, G. W. Bryant, and J. Aizpurua, Phys. Rev. B **74**, 195339 (2006).
[32] R. Santoprete, B. Koiller, R. B. Capaz, P. Kratzer, Q. K. K. Liu, and M. Scheffler, Phys. Rev. B **68**, 235311 (2003).
[33] G. Bester, J. Shumway, and A. Zunger, Phys. Rev. Lett. **93**, 047401 (2004).
[34] Y. A. Bychkov and E. I. Rashba, J. Phys. C **17**, 6039 (1984).
[35] A. V. Khaetskii, Phys. Rev. B **45**, 13777 (1992).
[36] Y. Kato, R. C. Myers, A. C. Gossard, J. Levy, and D. D. Awschalom, Science **299**, 1201 (2003).
[37] C. F. Destefani and S. E. Ulloa, Phys. Rev. B **71**, 161303 (2005).
[38] T. Andlauer and P. Vogl, Phys. Rev. B **79**, 045307 (2009).
[39] J. Y. Fu and M. W. Wu, J. Appl. Phys. **104**, 093712 (2008).
[40] W. H. Kuan, C. S. Tang, and W. Xu, J. Appl. Phys. **95**, 6368 (2004).
[41] E. Tsitsishvili, G. S. Lozano, and A. O. Gogolin, Phys. Rev. B **70**, 115316 (2004).
[42] B. Lassen, M. Willatzen, D. Barettin, R. V. N. Melnik, and L. C. L. Y. Voon, J. Phys.: Conf. Ser. **107**, 012008 (2008).
[43] COMSOL MULTIPHYSICS version 3.5a, www.comsol.com
[44] R. V. N. Melnik, Appl. Math. Comput. **107**, 27 (2000).
[45] R. V. N. Melnik and M. N. Moskalkov, Diff. Eq. **27**, 860 (1991).
[46] R. V. N. Melnik and K. N. Melnik, Appl. Math. Model. **24**, 147 (2000).
[47] R. V. N. Melnik and K. N. Zotsenko, Appl. Numer. Math. **48**, 41 (2004).
[48] X. Peng and P. Logan, Appl. Phys. Lett. **96**, 143119 (2010).
[49] I. M. Lifshits and L. M. Rosentsveig, Zh. Eksp. Teor. Fiz. **17**, 783 (1947).
[50] F. C. Buroni and A. Sáez, Proc. R. Soc. London, Ser. A **466**, 515 (2010).
[51] I. P. Ipatova, V. G. Malyshkin, and V. A. Shchukin, J. Appl. Phys. **74**, 7198 (1993).
[52] A. D. Andreev, J. R. Downes, D. A. Faux, and E. P. O'Reilly, J. Appl. Phys. **86**, 297 (1999).
[53] D. Barettin, B. Lassen, and M. Willatzen, J. Phys.: Conf. Ser. **107**, 012001 (2008).
[54] M. W. Bayerl, M. S. Brandt, T. Graf, O. Ambacher, J. A. Majewski, M. Stutzmann, D. J. As, and K. Lischka, Phys. Rev. B **63**, 165204 (2001).
[55] F. Bernardini and V. Fiorentini, Phys. Rev. B **57**, R9427 (1998).